In situ X-Ray Diffraction of Shock-Compressed Fused Silica

Sally June Tracy, Stefan J. Turneaure, and Thomas S. Duffy

In situ X-ray diffraction of shock-compressed fused silica

Sally June Tracy,[1] Stefan J. Turneaure,[2] and Thomas S. Duffy[1]

[1]*Department of Geosciences, Princeton University,*

Princeton, New Jersey 08544, U.S.A

[2]*Institute for Shock Physics, Washington State University,*

Pullman, Washington 99164-2816, U.S.A

Abstract

Due to its widespread applications in materials science, SiO_2 has been extensively examined under shock compression. Both quartz and fused silica transform through a so-called "mixed-phase region" to a dense, low compressibility high-pressure phase. For decades the nature of this phase has been a subject of debate. Proposed structures include crystalline stishovite, another high-pressure crystalline phase, or a dense amorphous phase. Here we use plate impact experiments and pulsed synchrotron X-ray diffraction to examine the structure of fused silica shock compressed to 63 GPa. In contrast to recent laser-driven compression experiments, we find that fused silica adopts a dense amorphous structure below 34 GPa. When compressed above 34 GPa, fused silica transforms to untextured polycrystalline stishovite. Our results can explain previously ambiguous features of the shock compression behavior of fused silica and are consistent with recent molecular dynamics simulations. Stishovite grain sizes are estimated to be ∼5-30 nm for compression over a few hundred nanosecond timescale.

Laboratory shock wave experiments have long played an important role in the study of materials in extreme environments. Shock compression experiments provide the unique capability to study impact phenomena in real time and allow for measurements of equations of state [1–3], phase transitions [4, 5], melting [6–9], sound velocities [5, 10, 11], Grüneisen parameter [12, 13], and transport properties [14]. However, a limitation of shock wave studies is that the *in situ* crystal structure of high-pressure phases formed under dynamic compression is generally not known.

Due to its fundamental importance in condensed matter physics and geophysics, SiO_2 is one of the most intensely studied materials under high-pressure conditions. Fused silica is widely used as an optical material and the its dynamic response is needed to understand high-powered laser-matter interactions and ballistic penetration [15–18]. SiO_2 is used as a model system for understanding the physics of amorphous materials at high pressures [19]. In addition, SiO_2 is the most abundant oxide constituent of the Earth's crust and serves as an archetype for silicate crystals and melts of the deep Earth. As a result, the behavior of silica under dynamic loading is essential for modeling the effects of impacts and explosions in the crust. Despite its wide application, existing models of the dynamic response of SiO_2 [20–23] suffer from limitations arising from uncertainties about the structure of the high-pressure phase(s).

Based on pressure-density Hugoniot measurements, the shock compression behavior of fused silica can be divided into three regions: 1) an elastic regime extending to 8-9 GPa, 2) a highly compressible region from 10-35 known as the "mixed-phase region", and 3) a dense, low compressibility phase above 34 GPa. Despite decades of study, the nature of the crystal structure or structures existing in the mixed- and high-pressure regions are not known. It is often assumed that the high-pressure phase corresponds to crystalline stishovite (or its $CaCl_2$-type modification) as observed in static compression experiments and that the mixed-phase regime is a mixture of the low- and high-pressure forms [2, 23, 24], but direct proof is lacking. Luo et al. [20] have argued that shocked quartz transforms to stishovite (or a stishovite-like) phase between 15-46 GPa. Recent laser-driven compression experiments have suggested that stishovite may begin forming as low as 5 GPa [25]. Others have suggested that the high-pressure phase of SiO_2 corresponds to another high-pressure crystal structure [26, 27] or an amorphous phase [21, 28–33]. Recovery experiments generally find amorphous material with only trace quantities of stishovite [31, 34], but due to the high-temperature

release path it is an open question whether amorphization occurs during compression or release. The formation of stishovite requires transformation of an initially tetrahedrally coordinated glass to a dense, octahedrally coordinated crystalline structure at high pressures. It has been argued that this would require a reconstructive phase transformation that would be too sluggish to occur on shock wave timescales [30].

To probe the crystal structure of fused silica under shock compression, we carried out time-resolved X-ray diffraction (XRD) measurements coupled with gun-based dynamic compression. Plate impact loading provides uniform, well-defined conditions within the sample. The diffraction data are combined with continuum-level measurements to reveal a complete picture of the material response from the atomic length scale to the continuum level, allowing for the unambiguous determination of the phase(s) formed at ∼100 ns timescales from 12 to 63 GPa.

Plate impact experiments were carried out at the Dynamic Compression Sector of the Advanced Photon Source (APS). Planar shock waves in fused silica were generated using LiF impactors accelerated in a polycarbonate projectile to a velocity of 1.8–5.6 km/s using either a single-stage propellant gun or a two-stage light gas gun. A schematic of the impact configuration is shown in supplementary material (SM) figure S4 [35]. The resulting stress states in the sample ranged from 12 to 47 GPa. In one additional experiment, the fused silica sample was backed by a LiF window and a double-shock state reaching 63 GPa was produced by reshock from 46 GPa to 63 GPa at the LiF window. Experimental parameters are provided in the SM, Table S1 [35]. Laser interferometry was used to measure impact velocities and the continuum stress and density states were determined by impedance matching using the known equations of state of fused silica and LiF. *In situ* X-ray diffraction measurements were obtained using a single-bunch (∼100 ps) of the APS storage ring operated in 24-bunch mode. For each experiment, four X-ray diffraction images each separated by 153.4 ns were recorded. Experiments were designed such that one or two X-ray diffraction frames were obtained while the shock wave propagates through the fused silica but before it reaches the rear surface. The X-ray diffraction data for the frames corresponding to the most fully compressed material were analyzed in detail to determine the structure and state of the shock-compressed material. See supplementary material for further details [35].

Figure 1 shows a series of azimuthally integrated diffraction patterns obtained during uniform stress states ranging from 17 to 63 GPa. The diffraction patterns correspond to
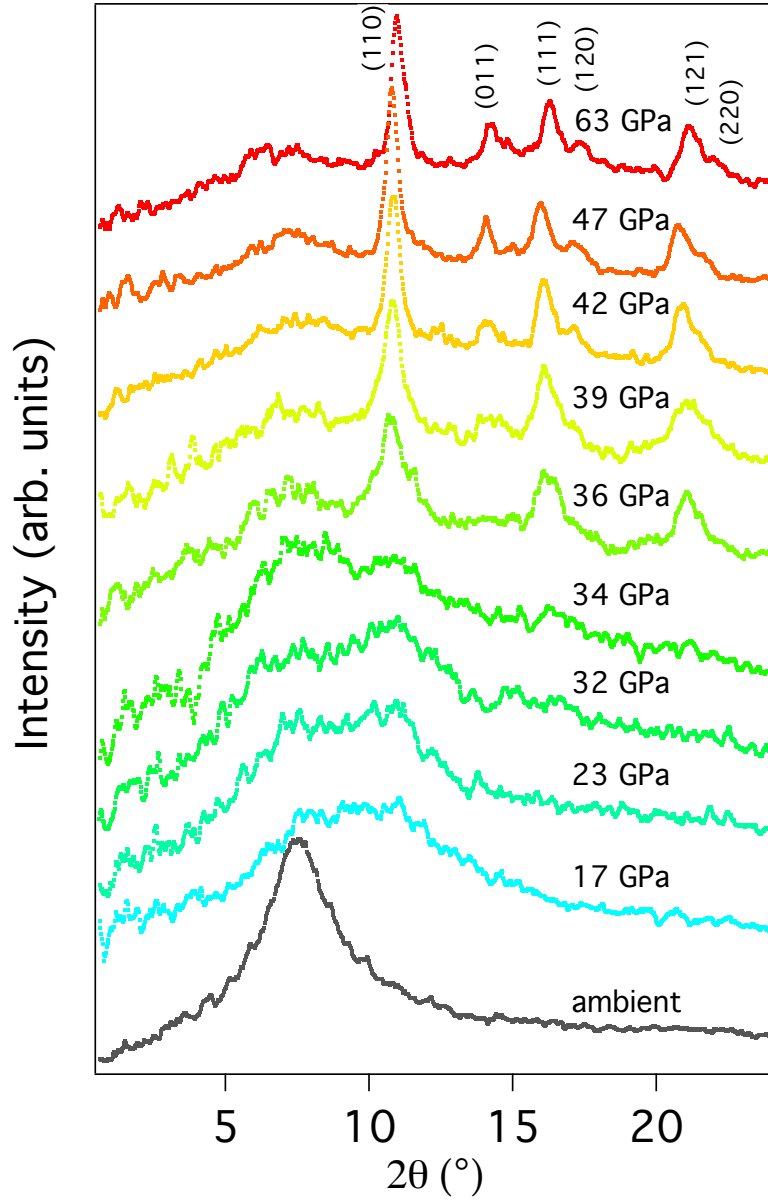
FIG. 1. Azimuthally integrated X-ray diffraction data collected for a series of plate impact experiments with peak stress states between 17 and 63 GPa. Stishovite peaks are labelled with *hkl* values.

frames captured during the uniform shock state prior to the shock front having traversed the entire thickness of the sample. Owing to the transmission geometry of the experiments (SM, Fig. S4 [35]), the measurements sample some amount of uncompressed SiO_2 and/or elastically compressed material. The fraction of uncompressed material was less than 8% for all patterns shown in Fig. 1 except for the one at 23 GPa, in which 22% of the SiO_2

remained uncompressed. An additional shot collected at 12 GPa is not shown in Fig. 1, as the fraction of uncompressed material was nearly 40%. The elastic precursor is overdriven at peak stresses above 25 GPa. Note also that the incident X-ray beam passes through the body of the polycarbonate projectile giving rise to additional amorphous scattering at low angle (SM, Figs. S6, S9 [35]).

At 34 GPa and below, no crystalline diffraction peaks from the sample were detected but diffuse scattering features were observed at two-theta values less than 15 degrees, indicating that fused silica remained amorphous when shock-compressed to these conditions (Fig. 1, SM, Fig. S9 [35]). At stresses of 36 GPa and above, we observe sharp diffraction peaks demonstrating that fused silica transformed to a crystalline phase (Fig.1, SM, Fig. S5 [35]). The diffraction rings are relatively smooth, indicating that the high-pressure phase does not have significant texture.

When compressed under static pressure, SiO_2 adopts a series of crystalline phases from quartz to coesite (C2/c) to stishovite (rutile structure, $P4_2/mnm$) to the $CaCl_2$-type phase (Pnnm) [48]. In addition, a number of metastable forms of SiO_2 have been observed experimentally or predicted theoretically [49]. To identify the phase crystallizing on the fused silica Hugoniot, we performed diffraction simulations that account for the shape of the pink X-ray beam (SM, S3.1 [35]). Figure 2 shows excellent agreement between the background-subtracted data and diffraction simulations using the rutile structure, demonstrating that fused silica transforms to stishovite upon shock compression above 34 GPa. Within the resolution of our measurements, there is no evidence for any peak splitting or enhanced broadening of the stishovite (120) and (121) peaks that would indicate a further transformation to a $CaCl_2$-type phase. Other possible high-pressure phases including coesite, α-PbO_2-type and Fe_2N-type [26, 27, 49] are not consistent with the observed diffraction data.

Our results allow us to explain previously ambiguous features of the behavior of fused silica under shock compression. Notably, the abrupt change in compressibility along the Hugoniot at 35 GPa corresponds precisely to where we identify the amorphous-crystalline phase change (Fig. 3). This is also consistent with *in situ* electrical conductivity measurements of fused silica [14] that reported a discontinuous decrease in resistivity at 35 GPa. More generally, our results show the viability of amorphous to crystalline phase transformations within the $\sim$100 ns timescale of plate-impact experiments.
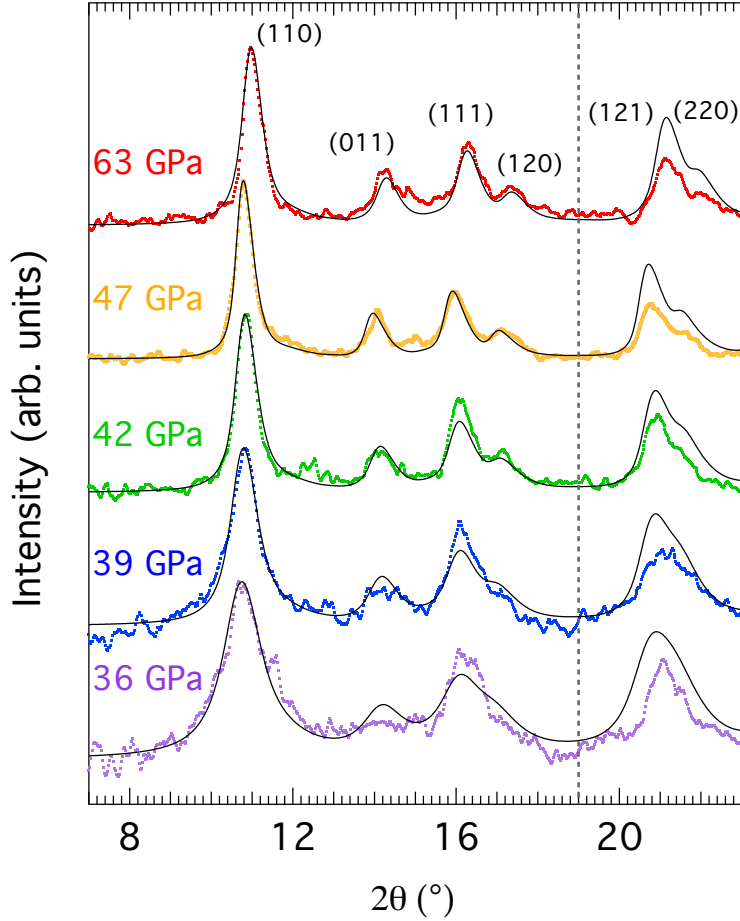
5

FIG. 2. X-ray diffraction data in the high-pressure region. The fits (black curves) overlay experimental data (points). Least-squares fits were preformed to determine the lattice parameters and peak widths for stishovite diffraction peaks. The vertical dotted line denotes the extent of the fit region, above which detector-sensitivity effects render intensity data quantitatively unreliable.

Figure 3 shows that the crystal densities determined from X-ray diffraction above 34 GPa are consistent with previous continuum Hugoniot data (Fig. 3). This figure includes a calculated Hugoniot for stishovite using a Mie-Grüneisen equation of state (SM, S4 [35]), demonstrating that our X-ray diffraction results are consistent with the expected properties of stishovite along the Hugoniot. The thermodynamic parameters used for the calculated Hugoniot curve in Fig. 3 are listed in SM, Table S3 [35].

Our results are also consistent with recent molecular dynamics simulations which report the conversion of fused silica to polycrystalline stishovite on timescales of a few nanoseconds
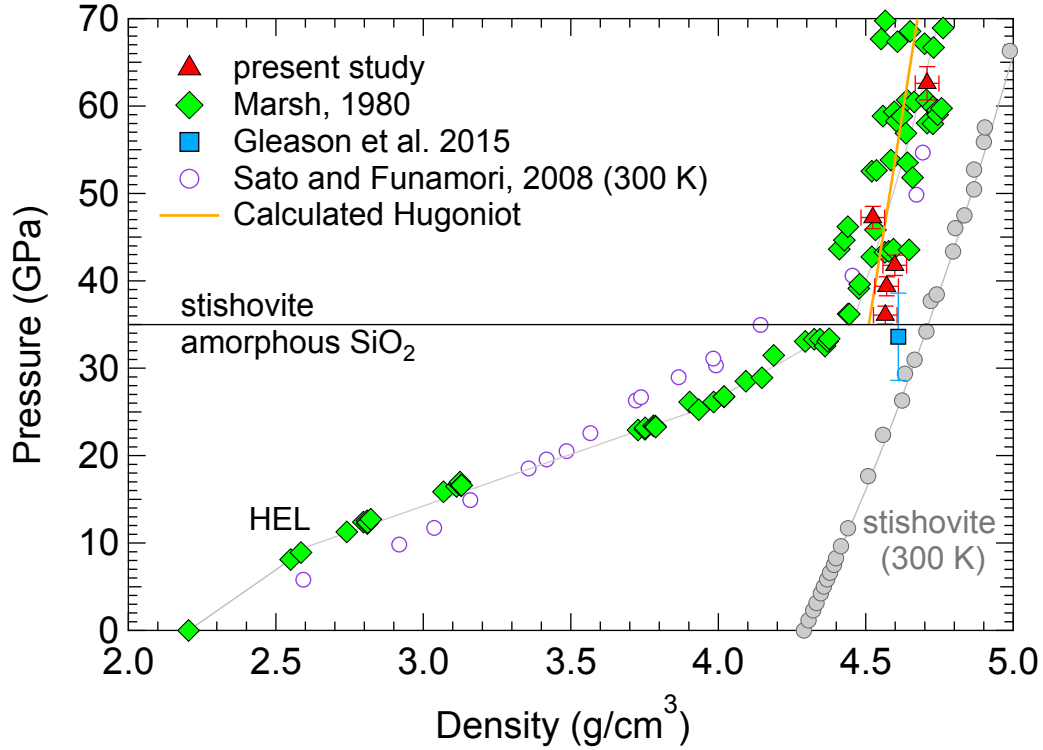
FIG. 3. Shock Hugoniot curve for fused silica. Red triangles show X-ray densities from this study. Continuum Hugoniot data from gun experiments [50] are shown as green diamonds along with X-ray density (blue square) determined from laser-driven compression [25]. Also shown are 300-K static compression data for stishovite (gray circles) [51] and fused silica (open purple circles) [52]. HEL= Hugoniot Elastic Limit.

at pressures above 50 GPa [53]. The transformation is described by a homogeneous nucleation and growth model involving only small-scale atomic motions with atomic neighbor memories largely erased in the transformation. The grain sizes inferred from our results are consistent with extrapolations of the molecular dynamics simulations from ∼1 ns to hundreds of nanoseconds, as described below.

We observe pronounced sharpening of the diffraction peaks between 36 and 47 GPa (Fig. 2). This is particularly evident for the strong stishovite (110) peak. This suggests grain growth is enhanced as temperature rises with increasing shock pressure. The degree of peak broadening was determined by convolving Lorentzian profiles with the diffraction simulations. Sample broadening was assessed after accounting for broadening from the X-ray source, instrumental broadening and broadening due to finite sample thickness (SM, S3

[35]). We attribute this broadening to grain size by applying the Scherrer equation to the full width at half maximum of the stishovite (110) peak using [54]:

$$\langle d \rangle = \frac{0.94\lambda}{\beta \cos(\theta)}. \tag{1}$$

Here $\langle d \rangle$ is the mean stishovite grain size, $\lambda = 0.539$ Å is the X-ray wavelength, β is the peak width, and θ is the Bragg angle. This equation provides a lower limit on the grain size of the transformed material in the shocked state. Figure 4 shows our results together with calculated grain sizes from molecular dynamics simulations of stishovite formed from shock-compressed fused silica [53].

In the simulations, thermal energy promotes the rapid nucleation of nanocrystals from local regions of coherent short-range order. This is followed by a grain coalescence phase where grain growth depends primarily on shock temperature. When shock compressed into the high-pressure region, fused silica first adopts a dense disordered structure. This intermediate structure is transient and within picoseconds local regions of order nucleate and transformation to a fine grained stishovite occurs in a matter of nanoseconds. The subsequent rate of grain growth is given by [53]:

$$\langle d \rangle = \left(\langle d_0 \rangle^3 + K\Delta t \right)^{1/3}, \tag{2}$$

$$K = K_0 \exp\left(\frac{-Q}{k_B T} \right). \tag{3}$$

Here $\langle d \rangle$ is the average grain size in nm, $\langle d_0 \rangle$ is the grain size at the start of the grain coalescence growth phase, Δt is the time after start of coalesce, k_B is Boltzmann's constant, and T is temperature. Δt was taken as the diffraction frame time relative to impact. Values for K_0, Q and $\langle d_0 \rangle$ are given in Ref. [53].

The uncertainty in our result arises primarily from uncertainty in shock temperature. Calculated single shock temperatures range from 3200-5800±500 K between 36 and 63 GPa. Double shock temperatures in this range are 2400-4300±K (SM, S4 [35]). Figure 4 shows that the grain sizes determined from our experiments at timescales of hundreds of nanoseconds are consistent with the model inferred from molecular dynamics simulations up to 1.5 ns.

Our results demonstrate that the region of the Hugoniot from 10-34 GPa is not a "mixed-phase region" but instead corresponds to densification of the starting glass (Figs. 1, 3). Under room-temperature compression, SiO_2 glass initially undergoes rearrangement of SiO_4

tetrahedra followed by a continuous change in coordination with increasing pressure, transforming to a dense, nearly octahedrally coordinated structure by about 35 GPa [52, 55]. We envision a similar process occurring in the shock-compressed glass. The amorphous structure seen in Figure 1 consists of two broad components, one at low angle which is insensitive to pressure and a second at higher angle that moves to higher two-theta values with compression. Below 34 GPa, this second amorphous feature is peaked at $Q \sim 2.2 \mathring{A}^{-1} \left(Q = \frac{4\pi}{\lambda} \sin \theta \right)$, consistent with the first strong diffraction peak of SiO_2 glass observed in static compression experiments in this pressure range [52, 55–57]. The low-angle feature seen in all shots at $2\theta \sim 7°$ is a combined result of scattering from the polycarbonate projectile along with scattering from any remaining uncompressed (or elastically compressed) SiO_2.

A comparison of static compression with continuum Hugoniot data shows that the density of glass at 300 K is generally similar to Hugoniot densities up to 34 GPa (Fig. 3). In fact, from 20-34 GPa, the density of the glass along the Hugoniot exceeds that under 300-K compression, despite the higher temperature of the Hugoniot states. This suggests that high-temperature compression allows for additional compression mechanisms, enabling the glass to achieve a denser state than it can at lower temperatures. This is consistent with static compression data for fused silica which show enhanced densification upon compression at high temperatures [58, 59].

Based on analogy with static compression, recovery experiments, and theoretical models, we infer that the shock-compressed glass at 34 GPa is a nearly six-coordinated glass with a high degree of "stishovite-like" short-range order [52, 60, 61]. This disordered phase may be similar to the intermediate structure seen at early times in molecular dynamics simulations [53]. Our calculated shock temperature at this pressure ($\sim$3100$\pm$500 K) is broadly consistent with previous shock temperature measurements on fused silica [6, 62, 63]. Above this temperature threshhold, the requisite thermal energy is available to overcome an activation barrier, promoting small atomic displacements required to transform the highly-coordinated glass into crystalline stishovite on shock-compression timescales. This type of transformation arises from local correlated motions of atoms as opposed to longer length scale diffusive rearrangements, allowing for the transformation to proceed to completion over short timescales.

Our results are in marked contrast to recent laser-compression experiments that reported evidence for the formation of stishovite from fused silica at pressures below 34 GPa on
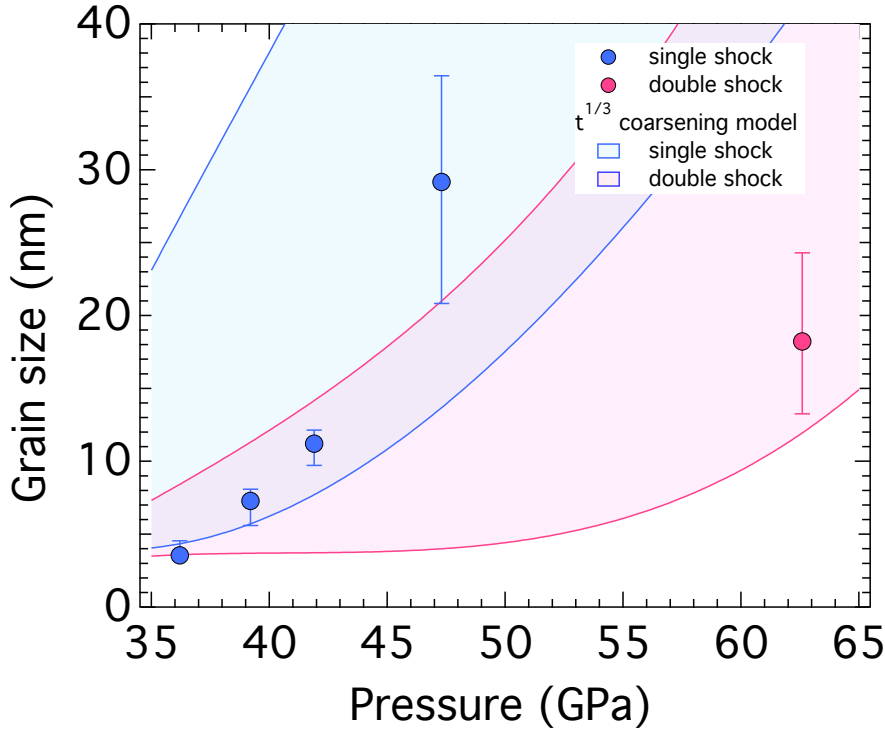
FIG. 4. Grain sizes determined using Scherrer equation from the current dexperiments (circles) along with range of grain sizes predicted using the $t^{1/3}$ coarsening law from molecular dynamics [53] for both single shock (blue field) and double shock (pink field) states. The large uncertainties in grain size calculations arise primarily from uncertainty in shock temperature.

nanosecond timescales [25, 64]. While the highest pressure datum in that study (34 ±5 GPa) overlaps our results, stishovite peaks were also observed at 19 GPa and below where we observe only amorphous material despite two orders of magnitude longer compression time. In the experiments of Refs. [25, 64], pressures were estimated only indirectly from measurements of the transit time through the entire sample package. The reported pressures may be significantly underestimated (see Ref. [25], SM, p. 9). Laser shock experiments may suffer from stress non-uniformity and non-steadiness of the shock wave. In contrast, plate impact experiments produce well-defined, planar and steady states of compression. The stress states in our sample are well-constrained by the precisely measured impact velocities and the known equations of state of fused silica and lithium fluoride. The consistency of our results with Hugoniot and other continuum data also provides strong support for our measurements.

Our study resolves the long controversy about the nature of the fused silica Hugoniot. Upon shock compression above the elastic limit up to 34 GPa, stishovite adopts a dense amorphous structure, comparable to its behavior under static compression. At shock pressures above 34 GPa, fused silica transforms to polycrystalline stishovite, consistent with the sharp change in the compressibility of the Hugoniot curve at this pressure. Stishovite grain sizes inferred from diffraction peak widths are consistent with the extrapolation of results from molecular dynamics simulations which identify a homogenous nucleation and two-stage grain growth model for the formation of stishovite under shock compression. Our results demonstrate that it is only above 34 GPa that there is the requisite thermal energy to drive crystallization and the region between 9 and 34 GPa represents a densification region rather than a true mixed-phase region, across which the glass evolves from a four- to six-coordinated structure.

---

[1] R. G. McQueen, S. P. Marsh, and J. N. Fritz, Journal of Geophysical Research **72**, 4999 (1967).

[2] J. A. Akins and T. J. Ahrens, Geophysical Research Letters **29**, 1394 (2002).

[3] Y. Zhang, T. Sekine, H. He, Y. Yu, F. Liu, and M. Zhang, Geophysical Research Letters **41**, 4554 (2014).

[4] J. L. Mosenfelder, P. D. Asimow, D. J. Frost, D. C. Rubie, and T. J. Ahrens, Journal of Geophysical Research: Solid Earth **114**, B01203 (2009).

[5] J. M. Brown and R. G. McQueen, Journal of Geophysical Research: Solid Earth **91**, 7485 (1986).

[6] G. A. Lyzenga, T. J. Ahrens, and A. C. Mitchell, Journal of Geophysical Research: Solid Earth **88**, 2431 (1983).

[7] J. H. Nguyen and N. C. Holmes, Nature **427**, 339 (2004).

[8] Q. Williams, R. Jeanloz, J. Bass, B. Svendsen, and T. J. Ahrens, Science **236**, 181 (1987).

[9] J. A. Akins, S.-N. Luo, P. D. Asimow, and T. J. Ahrens, Geophysical Research Letters **31**, L14612 (2004).

[10] H. Huang, Y. Fei, L. Cai, F. Jing, X. Hu, H. Xie, L. Zhang, and Z. Gong, Nature **479**, 513 (2011).

[11] T. S. Duffy and T. J. Ahrens, Journal of Geophysical Research: Solid Earth **100**, 529 (1995).

[12] C. W. Thomas and P. D. Asimow, Journal of Geophysical Research: Solid Earth **118**, 5738 (2013).

[13] S.-N. Luo, J. L. Mosenfelder, P. D. Asimow, and T. J. Ahrens, Geophysical Research Letters **29**, 1691 (2002).

[14] K. Kondo, A. Sawaoka, and T. J. Ahrens, Journal of Applied Physics **52**, 5084 (1981).

[15] F. Barmes, L. Soulard, and M. Mareschal, Physical Review B **73**, 224108 (2006).

[16] A. Salleo, S. T. Taylor, M. C. Martin, W. R. Panero, R. Jeanloz, T. Sands, and F. Y. Genin, Nature Materials **2**, 796 (2003).

[17] L. Hallo, A. Bourgeade, C. Mezel, G. Travaille, D. Hebert, B. Chimier, G. Schurtz, and V. T. Tikhonchuk, Applied Physics A- Materials Science & Processing **92**, 837 (2008).

[18] M. Grujicic, J. S. Snipes, and S. Ramaswami, Journal of Materials Engineering and Performance **25**, 995 (2016).

[19] C. S. Alexander, L. C. Chhabildas, W. D. Reinhart, and D. W. Templeton, International Journal of Impact Engineering **35**, 1376 (2008).

[20] S.-N. Luo, T. J. Ahrens, and P. D. Asimow, Journal of Geophysical Research: Solid Earth **108**, 2421 (2003).

[21] S. L. Chaplot and S. K. Sikka, Physical Review B **61**, 11205 (2000).

[22] H. Tan and T. J. Ahrens, Journal of Applied Physics **67**, 217 (1990).

[23] J. C. Boettger, Journal of Applied Physics **72**, 5500 (1992).

[24] R. G. McQueen, J. N. Fritz, and S. P. Marsh, Journal of Geophysical Research **68**, 2319

(1963).

[25] A. E. Gleason, C. A. Bolme, H. J. Lee, B. Nagler, E. Galtier, D. Milathianaki, J. Hawreliak, R. G. Kraus, J. H. Eggert, D. E. Fratanduono, G. W. Collins, R. Sandberg, W. Yang, and W. L. Mao, Nature Communications **6**, 8191 (2015).

[26] T. Sekine, M. Akaishi, and N. Setaka, Geochimica et Cosmochimica Acta **51**, 379 (1987).

[27] L. C. Chhabildas and D. E. Grady, in *Shock Waves in Condensed Matter-1983*, edited by J. R. Asay, R. A. Graham, and G. K. Struab (Elsevier, 1984) pp. 175–178.

[28] W. R. Panero, L. R. Benedetti, and R. Jeanloz, Journal of Geophysical Research: Solid Earth **108**, 2015 (2003).

[29] F. Langenhorst, Earth and Planetary Science Letters **128**, 683 (1994).

[30] F. Langenhorst and A. Deutsch, Elements **8**, 31 (2012).

[31] T. G. Sharp and P. S. DeCarli, in *Meteorites and the Early Solar System II*, edited by D. S. Lauretta and H. Y. McSween (University of Arizona Press, 2015) pp. 653–677.

[32] A. J. Gratz, W. J. Nellis, J. M. Christie, W. Brocious, J. Swegle, and P. Cordier, Physics and Chemistry of Minerals **19**, 267 (1992).

[33] N. M. Kuznetsov, in *High-Pressure Shock Compression of Solids VII.*, edited by V. E. Fortov, L. V. Alt'shuler, R. F. Trunin, and A. I. Funtikov (Springer New York, 2015) pp. 275–295.

[34] P. Berterretche, T. de Ressguier, M. Hallouin, and J. P. Petitet, Journal of Applied Physics **96**, 4233 (2004).

[35] See Supplemental Material at [URL will be inserted by publisher] for details concerning experimental procedure, data reduction and analysis, which includes Refs. [36-47].

[36] L. M. Barker and R. E. Hollenbach, Journal of Applied Physics **43**, 4669 (1972).

[37] O. T. Strand, D. R. Goosman, C. Martinez, T. L. Whitworth, and W. W. Kuhlow, Review of Scientific Instruments **77**, 083108 (2006).

[38] T. J. Ahrens, in *Geophysics, Methods in Experimental Physics*, Vol. 24, edited by G. H. Sammis and T. L. Henyey (Academic Press, 1987) pp. 185 – 235.

[39] Q. Liu, X. Zhou, X. Zeng, and S. N. Luo, Journal of Applied Physics **117**, 045901 (2015).

[40] T. Sun and K. Fezzaa, Journal of Synchrotron Radiation **23**, 1046 (2016).

[41] A. P. Hammersley, S. O. Svensson, M. Hanfland, A. N. Fitch, and D. Hausermann, High Pressure Research **14**, 235 (1996).

[42] R. G. McQueen, S. P. Marsh, J. W. Taylor, J. N. Fritz, and W. J. Carter, in *High Velocity*

Impact Phenomena, edited by R. Kinslow (Academic Press, New York, 1970) pp. 294–417.

[43] F. Jiang, G. D. Gwanmesia, T. I. Dyuzheva, and T. S. Duffy, Physics of the Earth and Planetary Interiors **172**, 235 (2009).

[44] R. A. Robie and D. R. Waldbaum, in *Geological Survey Bulletin 1259* (U.S. Govt. Print. Off., 1968).

[45] G. F. Davies, Journal of Geophysical Research **77**, 4920 (1972).

[46] J. R. Smyth and T. C. McCormick, in *Mineral Physics and Crystallography: A Handbook of Physical Constants*, edited by T. J. Ahrens (American Geophysical Union, Washington, D. C., 1995) pp. 1–17.

[47] Y. Sumino and O. L. Anderson, in *Handbook of Physical Properties of Rocks (1984), Volume 3*, edited by R. S. Carmichael (CRC Press, 1984) p. 94.

[48] R. J. Hemley, C. T. Prewitt, and K. J. Kingma, Reviews in Mineralogy and Geochemistry **29**, 41 (1994).

[49] L. S. Dubrovinsky, N. A. Dubrovinskaia, V. Prakapenka, F. Seifert, F. Langenhorst, V. Dmitriev, H.-P. Weber, and T. L. Bihan, Physics of the Earth and Planetary Interiors **143-144**, 231 (2004).

[50] S. P. Marsh, *LASL Shock Hugoniot Data* (University of California Press, Los Angeles, 1980, 1980).

[51] D. Andrault, R. J. Angel, J. L. Mosenfelder, and T. Le Bihan, American Mineralogist **88**, 301 (2003).

[52] T. Sato and N. Funamori, Physical Review Letters **101**, 255502 (2008).

[53] Y. Shen, S. B. Jester, T. Qi, and E. J. Reed, Nature Materials **15**, 60 (2016).

[54] B. D. Cullity, *Elements of X-ray Diffraction* (Addison-Wesley, 1956) p. 381.

[55] C. J. Benmore, E. Soignard, S. A. Amin, M. Guthrie, S. D. Shastri, P. L. Lee, and J. L. Yarger, Physical Review B **81**, 054105 (2010).

[56] C. Prescher, V. B. Prakapenka, J. Stefanski, S. Jahn, L. B. Skinner, and Y. Wang, Proceedings of the National Academy of Sciences **114**, 10041 (2017).

[57] Y. Inamura, Y. Katayama, W. Utsumi, and K. Funakoshi, Physical Review Letters **93**, 015501 (2004).

[58] F. S. Elkin, V. V. Brazhkin, L. G. Khvostantsev, O. B. Tsiok, and A. G. Lyapin, Journal of Experimental and Theoretical Physics Letters **75**, 342 (2002).

[59] M. Guerette, M. R. Ackerson, J. Thomas, F. Yuan, E. B. Watson, D. Walker, and L. Huang, Scientific Reports , 15343 (2015).

[60] E. M. Stolper and T. J. Ahrens, Geophysical Research Letters **14**, 1231 (1987).

[61] O. Tschauner, S. N. Luo, P. D. Asimow, T. J. Ahrens, D. C. Swift, T. E. Tierney, D. L. Paisley, and S. J. Chipera, High Pressure Research **24**, 471 (2004).

[62] M. Millot, N. Dubrovinskaia, A. Cernok, S. Blaha, L. Dubrovinsky, D. G. Braun, P. M. Celliers, G. W. Collins, J. H. Eggert, and R. Jeanloz, Science **347**, 418 (2015).

[63] H. Sugiura, K. Kondo, and A. Sawaoka, Journal of Applied Physics **53**, 4512 (1982).

[64] A. E. Gleason, C. A. Bolme, H. J. Lee, B. Nagler, E. Galtier, R. G. Kraus, R. Sandberg, W. Yang, F. Langenhorst, and W. L. Mao, Nature Communications **8**, 1481 (2017).